Wind and Structures, Vol. 3, No. 3 (2000) 159-175
DOI: http://dx.doi.org/10.12989/was.2000.3.3.159

Wavelet-based detection and classification of roof-corner pressure transients

Chris L. Pettit†

Air Force Research Laboratory, Wright-Patterson AFB, OH 45433-7532, U.S.A.

Nicholas P. Jones‡ and Roger Ghanem‡†

Department of Civil Engineering, The Johns Hopkins University, Baltimore, MD 21218, U.S.A.

Abstract. Many practical time series, including pressure signals measured on roof-corners of low-rise buildings in quartering winds, consist of relatively quiescent periods interrupted by intermittent transients. The dyadic wavelet transform is used to detect these transients in pressure time series and a relatively simple pattern classification scheme is used to detect underlying structure in these transients. Statistical analysis of the resulting pattern classes yields a library of signal "building blocks", which are useful for detailed characterization of transients inherent to the signals being analyzed.

Key words: wavelet transform; transients; detection; classification

1. Introduction

Recent applications of the wavelet transform in wind engineering have focused on detecting gusts and quantifying intermittency in the atmospheric surface layer (ASL). Gurley and Kareem (1995) use the wavelet transform for spectral density estimation and simulation of stochastic processes, such as wind speed, based on a given nonstationary record of that process. Their approach is used to generate an ensemble of signals whose statistics resemble those of the parent process. Dunyak and his colleagues (1998, 1997) have published several papers regarding the detection of coherent structures through statistical analysis of wavelet-transformed wind speed measurements. Jordan *et al*. (1996) use the wavelet transform to reveal the pronounced intermittency of particular wavelet scales in field measurements of longitudinal velocity fluctuations. Several papers presented at the *10th International Conference on Wind Engineering* (1999) feature additional wavelet-based efforts by these and other authors to quantify the intermittency of wind speed measurements.

An equally important issue is the interaction of incident turbulence with building structures. Freestream turbulence and coherent structures often combine with building geometry to produce isolated severe suction peaks. A well-known example of this is the strong suction generated on the corners of low-rise building roofs in winds that approximately bisect the roof-corner angle (Lin,

† Research Aerospace Engineer, Air Vehicles Directorate(Formerly Graduate Research Assistant, The Johns Hopkins University)
‡ Professor
‡† Associate Professor

Surry and Tieleman 1995). This type of flow generates a pair of relatively stable, conical vortices reminiscent of those observed over delta wings in aeronautical applications. Moreover, turbulence in the ASL causes these vortices to fluctuate both in strength and in axial direction. Tieleman *et al.* (1994) describe this flow and the associated severe roof-corner pressure transients. Jordan *et al.* (1996) suggest that the intermittent character of certain wavelet scales ought to correlate with these peak suction pressures, but do not provide quantitative verification of this hypothesis.

The extreme local loads associated with these transients must be accounted for in structural design; therefore, the intermittent peak loads need to be quantified and the physical mechanisms responsible for their generation need to be fully understood. However, detailed analysis of these peaks is complicated by their transient nature.

The work described herein provides a framework for detecting and characterizing these pressure transients. The wavelet transform is used to account for the nonstationary nature of these processes because it permits the use of analysis functions that are better adapted than sinusoidal functions to analyzing transient features in a signal. Whereas traditional spectral analysis smears the details of transients across a wide frequency range and buries their temporal location in the relative phase angle of the frequency components, the wavelet transform decomposes a time history onto a family of self-similar, localized functions that span the joint time-scale (or time-frequency) plane. Through this approach, transients are characterized by their wavelet coefficients at each time step and scale.

To better quantify the types of transients, as well as their rates of occurrence, that exist in wind pressure measured at a particular location on a structure, the signal can be examined to extract characteristic peaks associated with significant transients. Transients related to a particular flow mechanism are expected to exhibit consistent temporal structure. For example, individual vortices behind a circular cylinder are practically indistinguishable when viewed as a grouping of separate entities; thus, they can be said to constitute an equivalence class. This underlying structure can be quantified using pattern recognition techniques, so that a library of "building blocks" for characterizing and simulating intermittent pressure signals can be assembled.

The paper emphasizes the use of these concepts to detect and characterize extreme pressure transients, which are classified through their basic geometric features. Nonparametric probability density estimates are used to summarize transient arrival intervals and to quantify the statistical variation of members within each class of transients. Validation of the detection algorithm has been describe previously (Pettit *et al.* 1998). This was accomplished by analyzing time series composed of artificial transients contaminated by white noise. The current paper describes the analysis of pressure signals measured on the roof-corner of a low-rise building.

2. Theory

The primary steps executed by the transient detection and classification algorithm described in this paper are: (1) denoise the raw signal, (2) perform multiscale pattern detection, (3) compute a feature vector for each pattern, and (4) use clustering in feature space to detect underlying structure in the transients. When viewed as a whole, the algorithm conducts conditional sampling based on wavelet coefficients to extract and classify transients. After the transients are classified, a non-parametric probabilistic description of the geometric features of each class is generated using a standard kernel-based density estimation technique. Important features summarized in this manner include the duration and magnitude of each transient, as well as the number and location of prominent peaks that dominate their global structure.

2.1. Continuous and discrete wavelet transforms

There now exists an extensive collection of available texts on wavelet transform theory. Daubechies (1992) , Kaiser (1994), and Mallat (1998) are standard references that cover the theory in great detail, whereas Ogden (1997) provides a compact, lucid account that also discusses statistical applications.

The goal of wavelet analysis is to resolve the local behavior of a signal, $x(t) \in L^2(R)$, onto a set of localized, oscillatory functions called wavelets. These wavelets are derived from a mother wavelet, $h(t)$, through translation and dilation :

$$h_b^{(a)}(t) = \frac{1}{|a|^{1/2}} h\left(\frac{t-b}{a}\right) \tag{1}$$

where $h \in C$ and $(a, b) \in R^2$ in general. Translation by the parameter b detects the central location of distinct events in a signal. Dilation by the parameter a accounts for their extent or scale (in the sense of geographic maps).

The continuous wavelet transform (CWT) of $x(t)$ is

$$\tilde{x}(a, b) = (h_b^{(a)}(t), x(t)) = \int_{-\infty}^{\infty} \bar{h}_b^{(a)}(t) x(t) dt \tag{2}$$

where the overbar denotes the complex conjugate. This transform is operationally similar to the Fourier transform; qualitatively, scale is inversely proportional to frequency. The CWT can be inverted to yield a synthesis formula very similar to the inverse Fourier transform; hence, $x(t)$ may be recovered from

$$x(t) = \frac{1}{C_h} \int_0^{\infty} \int_{-\infty}^{\infty} (h_b^{(a)}(t), x(t)) h_b^{*(a)}(t) db \frac{da}{a^2} \tag{3}$$

where

$$C_h = 2 \int_0^{\infty} \frac{\hat{h}(w)}{w} dw \tag{4}$$

is a normalization factor that arises while inverting the continuous wavelet transform, and the carat ($\hat{}$) indicates the Fourier transform. The asterisk superscript (*) indicates the family of wavelets that is dual to the original family (Kaiser 1994). Note that Eq. (4) indicates that an admissible wavelet must have zero mean value (i.e., it must be oscillatory); otherwise C_h will not be finite and the transform will not be invertible.

When scale information in $\tilde{x}(a, b)$ is available only for smaller scales, $a < a_0$, recovery of x requires a complementary set of information corresponding to $\tilde{x}(a, b)$ for $a > a_0$. This is obtained by introducing a scaling function (Mallat 1998), g, that is an aggregation of wavelets at scales larger than 1. From this perspective, reconstruction may be understood qualitatively as an assembly of lowpass (scaling function) and highpass (wavelet) components. This is particularly evident in the Haar wavelet and its scaling function, which are described below.

The representation of $x(t)$ in Eq. (3) is highly redundant, in that it is a mapping from the real line to the real plane; that is, $t \in R$ and $(a, b) \in R^2$. A less redudant form of the wavelet transform is used here to improve the computational efficiency. This from is the dyadic wavelet transform (DyWT), in which the scale parameter is sampled at dyadic intervals; i.e., $a_m = 2^m$, where m is an

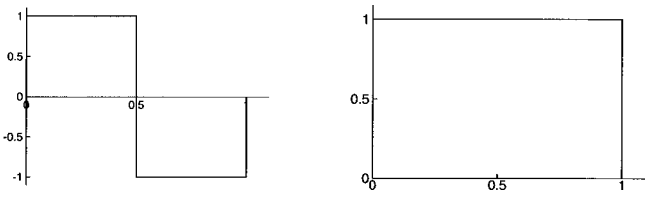

Fig. 1 The Haar wavelet

integer (Kadambe *et al*. 1992). Critical sampling in the time-scale plane is achieved by connecting the scale and translation parameters; the result is the wavelet series or discrete wavelet transform (DWT), which is especially useful in compression and filtering applications.

Multi-scale detection of transients (Section 2.2) is performed with the piecewise-constant Haar wavelet (Fig. 1), which is the most elementary member of a family of compactly-suppported wavelets formulated by Daubechies (1992) to satisfy certain polynomial reconstruction properties. The Haar wavelet and its associated scaling function are particularly well-suited to multi-scale edge detection because of their highly compact support and the fact that their shapes embody the most basic elements that define the geometry of transients: duration, magnitude, and abrupt changes.

2.2. Multi-scale discontinuity detection

Coherent transients, which are referred to here as patterns, are detected in a signal by their relatively sharp edges and high local curvatures. These abrupt transitions are detected in the DyWT as points with relatively large magnitude wavelet coefficients that are temporally contiguous across multiple scales (Mallat 1998, Strang and Nguyen 1996). The conceptual basis for this lies in the impulse response of the CWT or DyWT, which (analogously to the Fourier transform) exhibits energy at all scales (Fig. 2). Note that the DWT should not be used for pattern detection because it is not translation-invariant (Daubechies 1993); hence, a given pattern can generate different wavelet energy distributions depending on how its inherent scales align with the dyadic grid imposed by the DWT. This implies that the DWT's ability to detect a given transient would depend on its location

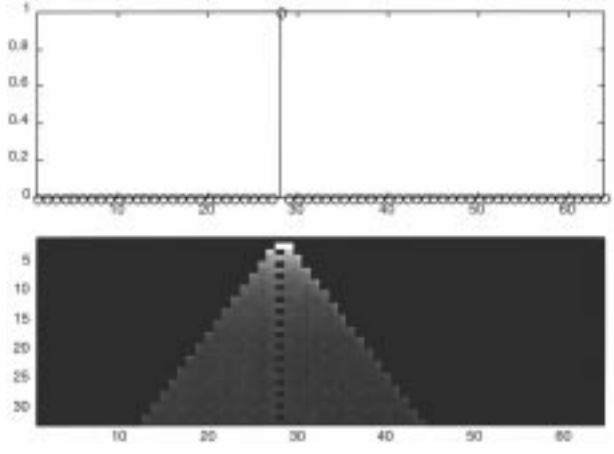

Fig. 2 Dirac impulse (at time index 28) and the corresponding region of influence in the time-scale plane

with respect to this dyadic grid; in constrast, the DyWT, while less efficient than the DWT, does not suffer from this weakness because it includes all available values of the translation parameter, *b*.

The signal is first denoised by thresholding the DWT; in essence, this is a localized low-pass filtering process (Strang and Nguyen 1996). Then the shorter scales in the Haar-based DyWT of the denoised signal are examined for localized values that exceed a pre-determined threshold across contiguous scales. In this way, the boundaries and extrema of individual transients, referred to as regions-of-sharp-change (rsc) are detected. Finally, empirically-devised criteria are applied to the signal segments between each pair of rscs to determine whether the segments correspond to true transients or to quiescent regions between transients. Space limitations preclude description of these criteria; an extensive discussion is given by Pettit (1998).

If regions of sharp change were detected using only the local modulus maxima of the wavelet coefficients instead of the multi-scale approach used here, the sharp changes detected would correspond to true edges, or singularities, in the signal. This is because the Haar wavelet has one vanishing moment, and Mallat (1998) shows that a wavelet $h(t)$ with k vanishing moments can be written as the k-th order derivative of a function $\theta(t)$, which can be shown to have fast decay in the time domain (i.e., $\theta(t)$ is localized). This property can be used to show that the corresponding wavelet transform based on $h(t)$ is equivalent to a multi-scale differential operator, which represents the k-th order derivative of the signal when it is convolved with $\theta(t)$. Because $\theta(t)$ has fast decay, this convolution yields a smoothed version of the original signal, so that for a wavelet with one vanishing moment (e.g., the Haar wavelet), the wavelet modulus maxima detect discontinuities. Because a threshold approach is used here, the sets of detected "edges" tend to be a mixture of regions having quasi-singular behavior (i.e., sharp increases or decreases in signal level) and regions of sharp curvature, such as transient peaks.

2.3. Pattern classification and recognition

The concept of pattern is accepted as a primitive from which a supporting theory is derived (Looney 1998); this concept has already been specialized for the current application to pressure transients. The goal of pattern recognition is to determine whether an object from population P belongs to a well-defined subpopulation or equivalence class S_n, such that $P = \cup_n^N S_n$. Hence, recognition is distinct from classification, in which we must decide if multiple patterns constitute an equivalence class. That is, classification is an inductive learning process whereas recognition is deductive.

In the current application, patterns are comprised of segments from discrete time signals; hence, they reside in a relatively high-dimensional vector space and are contaminated by noise. Both of these traits complicate the comparison of observed patterns. Classification and recognition therefore are implemented in a lower-dimensional feature space: a vector of feature components is computed for each pattern, and the relative similarity of each feature vector to the others is judged via a pre-determined metric. Selecting these features and the comparison metric is application-specific. The goal of feature selection is to summarize the essential nature of each pattern while simultaneously disregarding superfluous aspects, such as background noise.

2.4. Estimation of probability density functions

Nonparametric estimates of probability density functions (pdfs) are used extensively here to describe

the characteristics of detected pattern classes. Baxter and Beardah (1995) and Ogden (1997) provide useful summaries of the underlying theory and also provide references to more extensive texts on the subject.

The appproach used is essentially the standard kernel function method, in which a Gaussian kernel function is used to measure the local density of points in the chosen feature space. The feature space is discretized using a regular grid, with v denoting a point on this grid. For each grid point, a mountain function (Jang *et al*. 1997) is constructed :

$$m(\mathsf{v}) = \sum_{n=1}^{N_p} \exp\left(-\frac{\|\mathsf{v} - \boldsymbol{x}_n\|^2}{2\sigma^2}\right) \tag{5}$$

where $\boldsymbol{x}_n$ is an individual feature vector, N_p is the number of patterns detected (i.e., the number of feature vectors), and σ is and application-specific constant known as the kernel bandwidth, which controls the smoothness of the resulting mountain function. The pdf is then estimated by normalizing the mountain function to unit volume.

The choice of a proper kernel bandwidth value involves a certain degree of empiricism. Standard approaches are available (see Baxter and Beardah 1995) for selecting an appropriate bandwidth, and they were found (after the fact) to yield bandwidths recommendations similar to those chosen by trial and error.

3. Detection of pressure transients

3.1. Application to field measurements

The detection and classification algorithm described above has been applied successfully to signals consisting of artificial transients (Pettit *et al*. 1998). Next, the algorithm is applied to intermittent pressure time series measured on the roof-corner of a low-rise building. These data were obtained from the Wind Engineering Research Field Laboratory (WERFL) at Texas Tech University (TTU), which is described by Levitan and Mehta (1992). The work described herein concentrates on pressure measured with a three-by-three grid of transducers on the roof-corner (Fig. 3). Information regarding the type and exact location of each transducer is available in the references cited above.

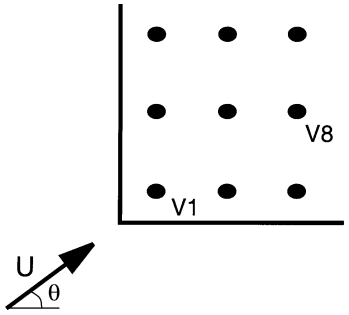

Fig. 3 Schematic of the transducer grid on the roof-corner of the Texas Tech WERFL. The wind direction approximately bisects the roof-corner angle

The results presented here are for two pressure time series recorded during a period in which the mean wind direction only approximately bisected the roof-corner angle ($\theta = 34.4^{o}$ in Fig. 3). The first signal is taken from the transducer closest to the roof corner, which is denoted as V1 in the WERFL documentation; the second is from transducer V8. Both signals were recorded during the same test.

The pressure signals consist of 36,000 points obtained at a sampling rate of 40 Hz. These data were provided as pressure coefficient time histories, which were computed by dividing each pressure value by the mean dynamic pressure observed over the entire recording period of fifteen minutes. For the present study, Signals V1 and V8 are truncated to 32,768 samples, and then denoised by thresholding the DWT. This pre-conditioning process, which essentially eliminates wavelet components with relatively small magnitudes, removes a sizable fraction of the background noise in the signals without noticeably reducing the magnitude or sharpness of the significant transients. Processing the resulting signals using the multi-scale detection algorithm produces a total of 67 transients in V1 and 89 in V8.

Preliminary visual examination of the detected transients indicated some potential for classification based on the number of suction peaks in smoothed versions of the transients. With this in mind, small-scale (noise-like) behavior in the patterns is decreased through the following steps:

1. Each pressure coefficient pattern is normalized such that its mean absolute value is unity and resampled to a duration of 50 samples. The normalization is implemented to compensate for difference between patterns that had similar shapes but different magnitudes. The resampling yields patterns with the same duration, so that the relative location of individual peaks in patterns can be stored as separate features. The original pattern's duration (before resampling) is also retained as a separate feature to be used in generating simulated time series (Pettit 1998).
2. The normalized and resampled patterns are then approximated using 12-th order Chebyshev polynomials. These approximate patterns generally provide good matches to the underlying

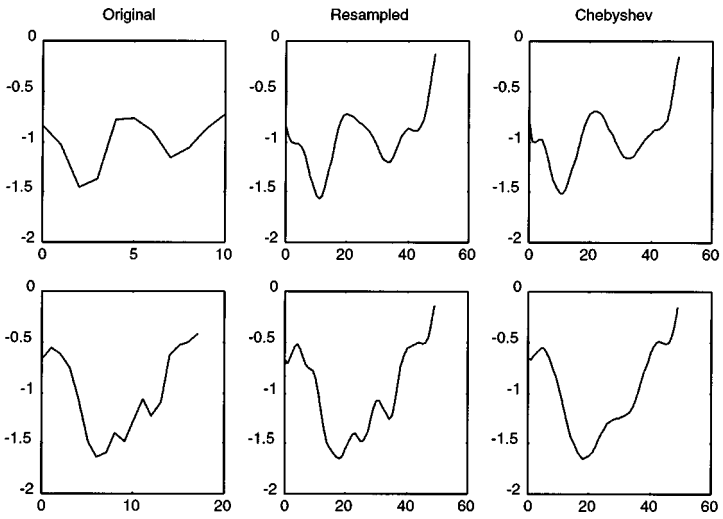

Fig. 4 Processing of two patterns detected in Signal V1. The first column contains the two original patterns, the second column shown the same patterns after resampling to a duration of 50 samples, and the third column depicts the 12th-order Chebyshev approximation of the resampled patterns

global shape of each pattern while simultaneously removing the local peaks that appear to correspond to incoherent turbulence, as opposed to coherent gusts.

The patterns are then classified according to the number of suction peaks in the smoothed patterns. Hence, the feature space upon which classification is based is one-dimensional and discrete. Also, as noted above, the duration and normalization factors are retained as separate features for subsequent analysis.

Fig. 4 illustrates the pattern-smoothing procedure for two patterns detected in V1. The first column of plots contains the original time series for each pattern, the second column depicts the resampled patterns, and the third column contains the Chebyshev approximations to the original patterns. From these smoothed patterns, the global suction peaks are counted. The top pattern in Fig. 4 is judged to have two suction peaks, and the bottom pattern is characterized as having a single suction peak. Peak counting is performed automatically by counting zero crossings in the first-order finite difference of each smoothed pattern.

3.2. Describing the shape of TTU patterns

After classifying the patterns according to the number of suction peaks, it was found useful to have an economical means of summarizing their basic shape that still retains important local geometric properties, such as the location and magnitude of each peak. This is achieved by imposing control points at the start, end, and local extrema of each smoothed pattern. Each suction peak is assumed to be bordered by a suction "valley" on both sides. This is illustrated for a generic two-peak pattern in the top portion of Fig. 5. For those peaks not bordered by a valley on one side, a

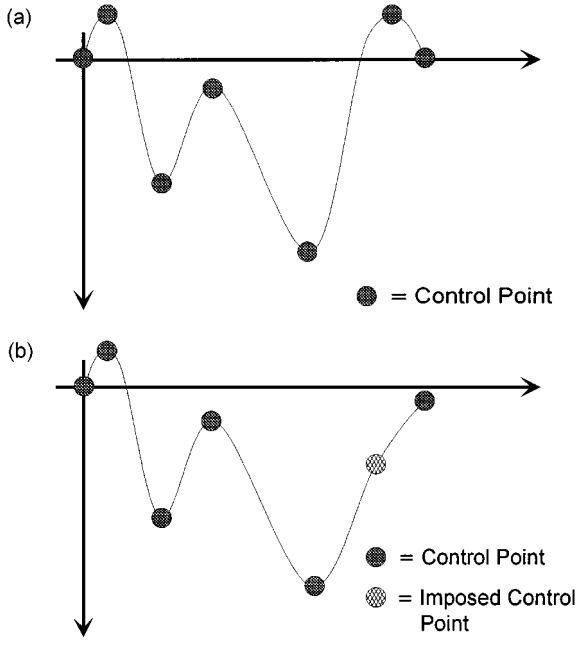

Fig. 5 (a) Control point locations for a generic transient pattern (b) Another generic transient, but with an imposed control point

control point is imposed as depicted in the bottom portion of Fig. 5. Each pattern in a number-of-peak class is thus assigned the same number of control points.

Because each smoothed pattern consists of the same number of samples and is scaled to unit mean absolute value, the time index and value of a particular control point, such as that corresponding to the first suction peak in the two-peak class, can be used to judge the relative similarity of the individual patterns within each class. In particular, if this peak happens to exhibit similar location and values in most of the patterns within each class, this indicates an additional degree of structure (i.e., beyond that indicated by the qualitative shape similarity) within the number-of-peaks class.

3.3. Results from the detection and classification algorithm

3.3.1. Signal V1

As noted earlier, 67 significant transients were detected in Signal V1. The top portion of Fig. 6 illustrates the original signal and a pattern indicator function, which is defined to be unity for those

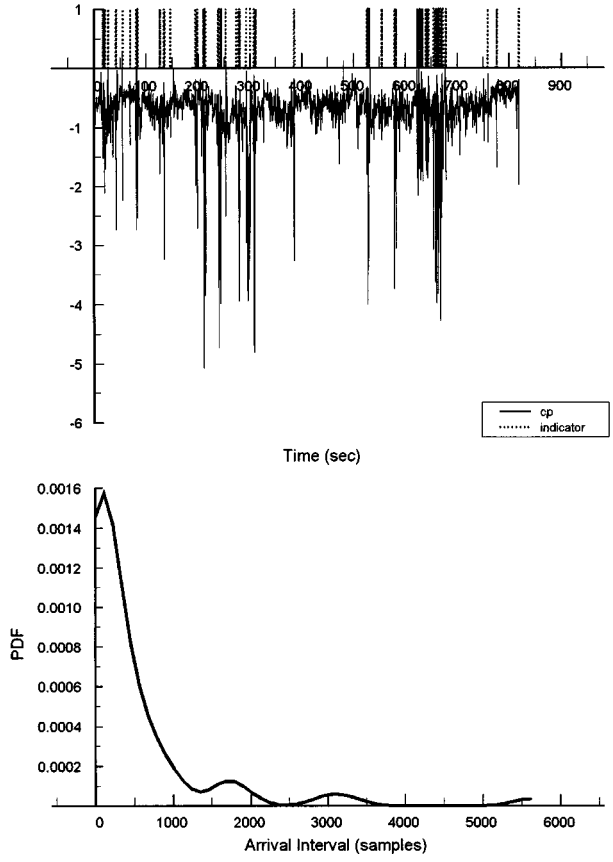

Fig. 6 (Top) Signal V1 and its pattern indicator function. (Bottom) Nonparametric arrival interval pdf estimate for Signal V1

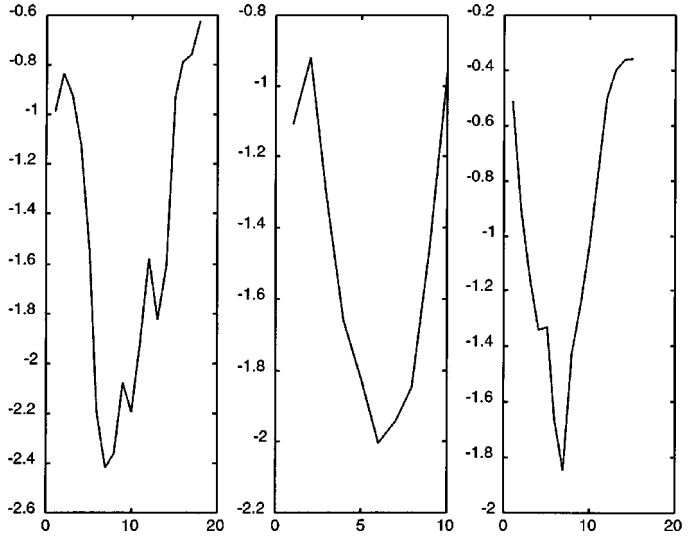

Fig. 7 Three single-peak patterns detected in Signal V1

time segments that contain a detected transient and zero otherwise. Note that the pattern indicator function exhibits good visual correlation with the clearly visible transients and also indicates that some noise-obscured transients are present.

The bottom frame of Fig. 6 contains a non-parametric estimate of the arrival-interval probability density function (pdf). The dominant primary peak in the pdf indicates that many of the transients occur in dense clusters and are separated by relatively short time intervals, whereas the smaller peaks reflect the longer, more quiescent periods between these clusters of transients.

Of the 67 patterns detected in Signal V1, 17 are found to have one suction peak, 33 have two suction peaks, and 17 have three suction peaks. Fig. 7 depicts three patterns that are judged to have a single suction peak. Although each of these patterns exhibits different local behavior from the others, they share a common underlying single-peak shape. Thus, they are classified together and their unique characteristics, such as their duration, peak value, and peak location, are stored as class-dependent features.

Fig. 8 and Fig. 10 display nonparametric probability density functions (pdfs) associated with several of these class-dependent features. The top frame in Fig. 8 shows a contour plot of the joint pdf of duration and magnitude scale factor for the single peak class in V1. The tight cluster of contours reflects the presence of a dominant peak in the pdf, which is more vividly illustrated in Fig. 9. This demonstrates that the majority of the single-peak patterns have similar duration and peak magnitude, and is indicative of additional underlying structure in the single-peak pattern class. That is, most of the patterns in this class have more in common than just a global shape characteristic; they also have similar magnitude and duration.

The second and third frames in Fig. 8 contain nonparametric pdfs for the magnitude of the start and end control points, respectively, of the single-peak transients in V1. The relatively large peak in each plot indicates that many of the normalized patterns in the single-peak class had similar beginning and ending values. This simply indicates that the mean value of the background signal (i.e., without the transients included) did not change significantly during the recording period.

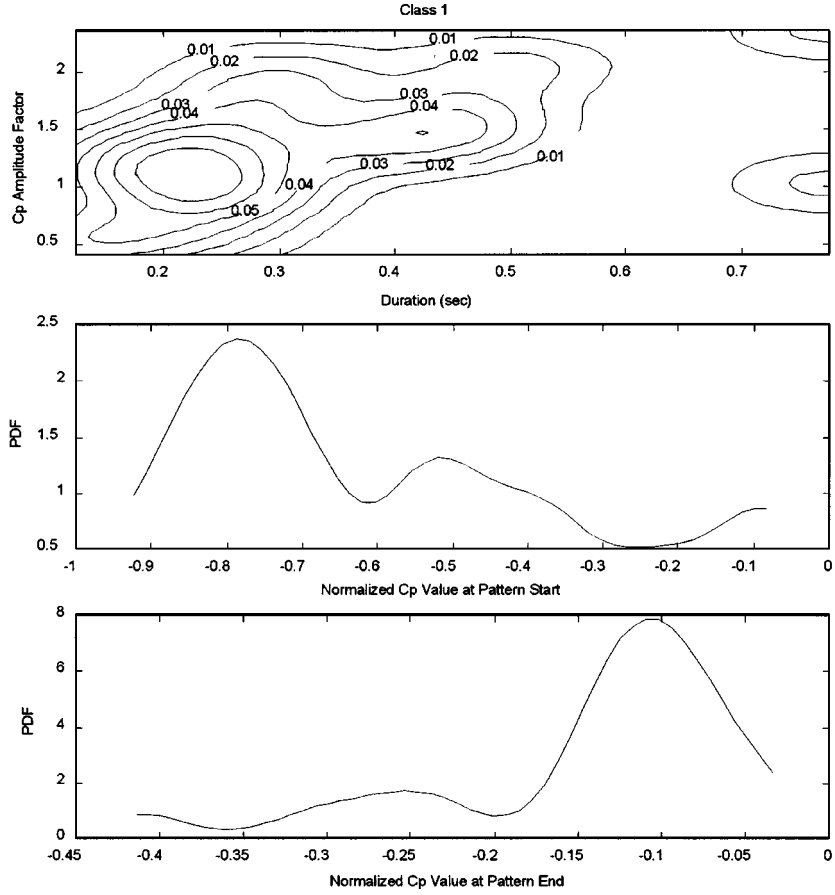

Fig. 8 (Top) Joint pdf of pattern duration and normalization factor for Signal V1: single-peak transients. (Center and bottom) Pdfs of start and end control point value.

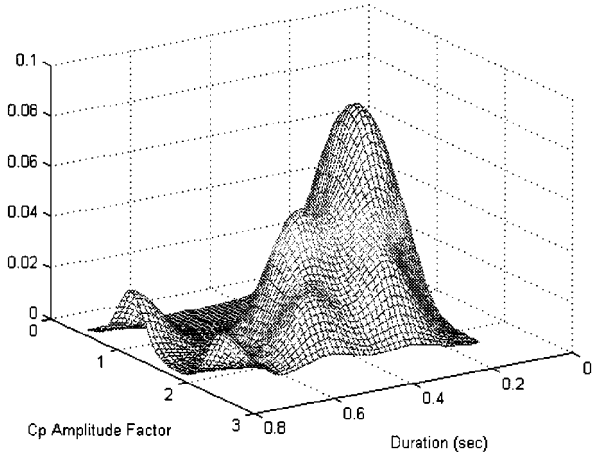

Fig. 9 Surface plot of the joint duration and C_p magnitude factor pdf. This plot corresponds to the contour plot in Fig. 8

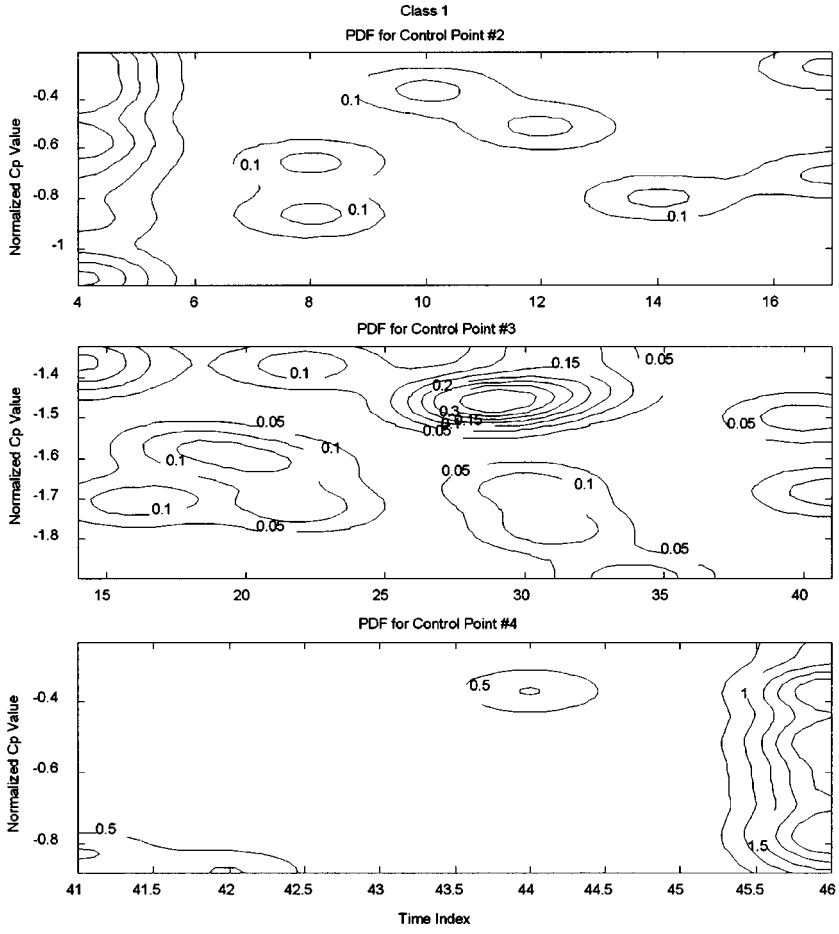

Fig. 10 Joint pdfs of intermediate control point time indices and values for Signal V1

The three contour plots in Fig. 10 portray the joint time index and value pdfs for the three intermediate control points corresponding to the normalized single-peak patterns in Signal V1. In particular, the center control-point pdf (middle frame of Fig. 10) corresponds to the single suction peak. The large peak indicated by the tight clusters simply reflects the structure noted above with regard to the duration and magnitude scale factors.

As noted above, approximately one-half of the transients detected in V1 (i.e., 33 out of 67 transients) have two suction peaks. The top frame in Fig. 11 shows that most of these patterns have similar duration and magnitude. This is a clear indication of some underlying similarity among the patterns in this class. Given that a similar degree of structure is present in the single-peak patterns, it appears that specific flow mechanisms are responsible for generating these transients.

3.3.2. Signal V8

Signal V8 (Fig. 12) contains several regions of intense activity, although signal levels are generally lower than for V1. This is attributed to the radial expansion of the approximately conical

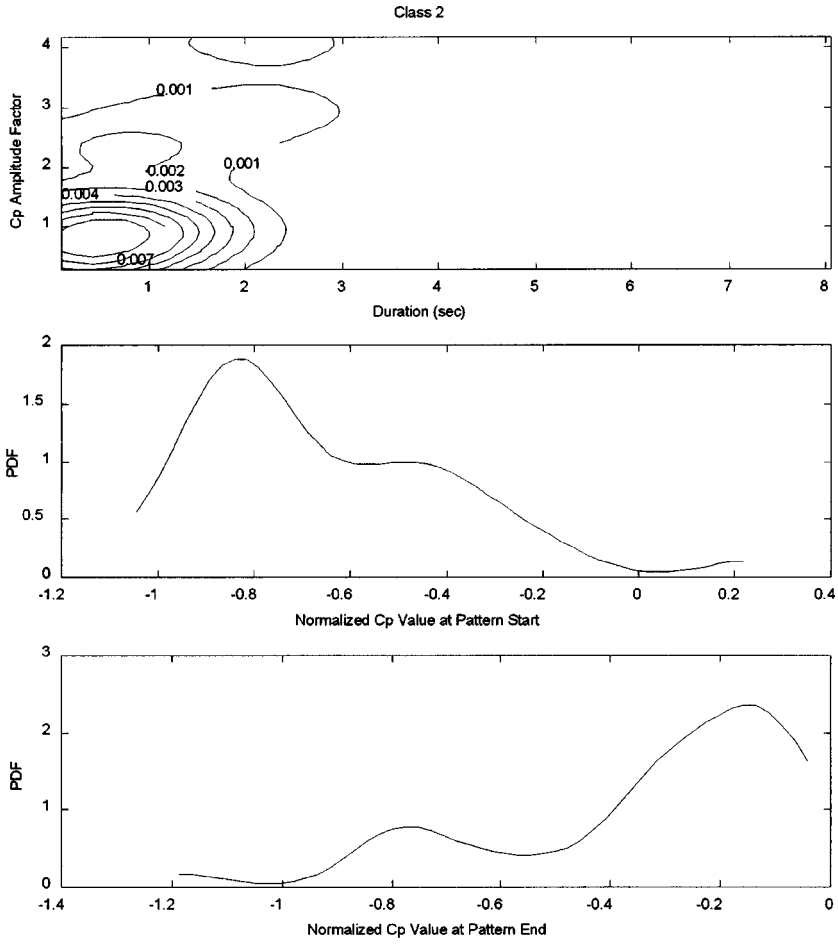

Fig. 11 (Top) Joint pdf of pattern duration and normalization factor for Signal V1: double-peak transients. (Center and Bottom) Pdfs of start and end control point value

corner vortices, which reduces streamline curvature, thereby decreasing the local suction. As in Signal V1, the transients tend to occur in bursts separated by quiescent periods; consequently, the arrival interval pdfs for Signals V1 and V8 are qualitatively similar. As noted previously, the pressure transients measured on the roof corner ought to correlate with coherent structures in the incident wind. There are significant challenges in trying to assess this correlation because the only incident wind measurements are taken 160 ft away from the building; hence, unless the anemometry tower happens to be situated on a direct line between the mean flow direction and the building, the detailed flow structure upstream of the building cannot be identified accurately.

Of the 89 transients detected in Signal V8, 20 are found to have a single suction peak, 43 have two peaks, 24 have three peaks, and two have four peaks. The relative distribution of patterns among the number-of-peak classes is similar to that for V1. Nonparametric pdfs for the control points of single-peak patterns in V8 are presented in Fig. 13 and Fig. 14. The tight cluster of contours in the first frame of Fig. 13 demonstrates that single-peak patterns in V8 tend to be of similar duration and magnitude. This trait was also noted earlier in Signal V1.

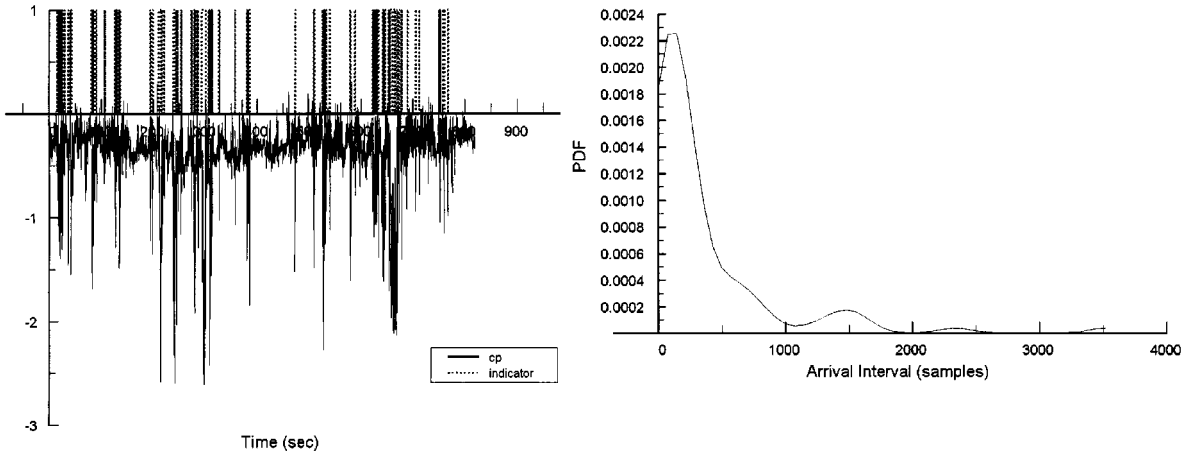

Fig. 12 (Top) Signal V8 and its pattern indicator function. (Bottom) Nonparametric arrival interval pdf estimate for Signal V8

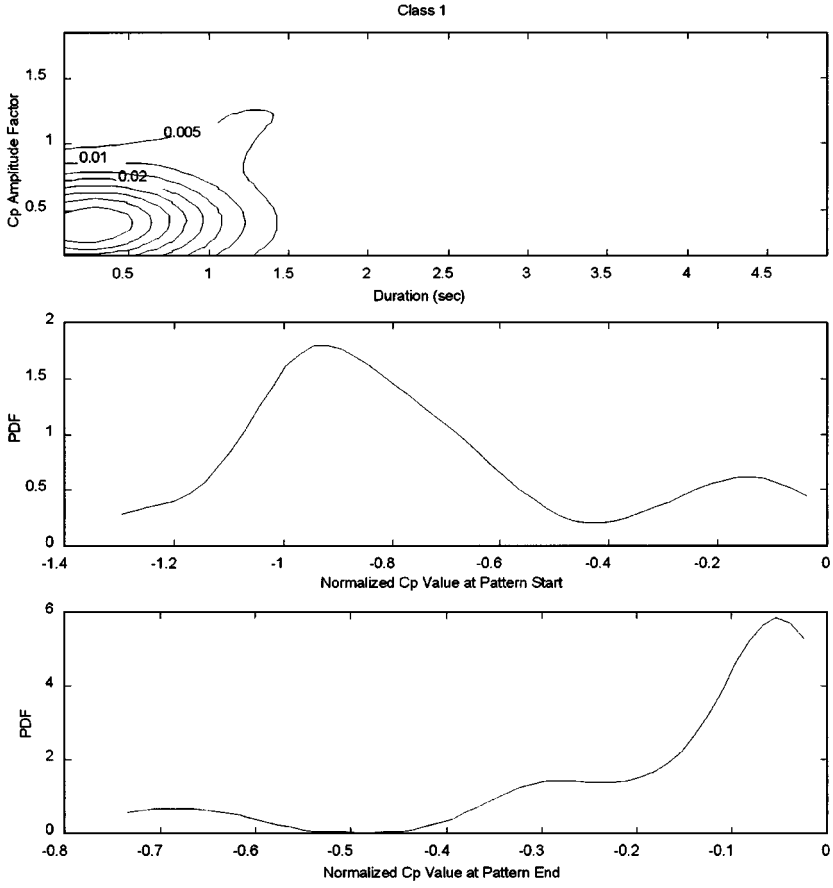

Fig. 13 (Top) Joint pdf of pattern duration and normalization factor for Signal V8. (Center and Bottom) Pdfs of start and end control point value

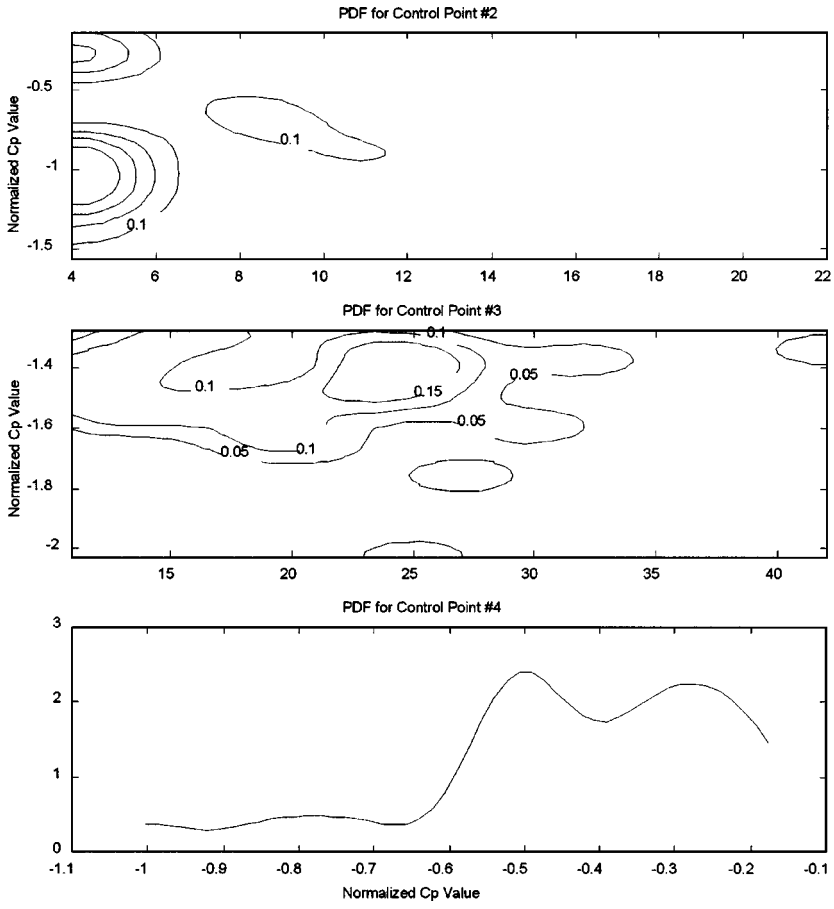

Fig. 14 Joint pdfs of intermediate control point time indices and values for Signal V8

Aside from the tight contour cluster in the top frame of Fig. 14, little additional structure is evident in the patterns from Signal V8. Although not described here, little structure was observed in Signal V6 transients, either. Physically, this can most likely be explained as follows. Transducers V6 and V8 are located on either side of the roof- corner bisector, which approximates the mean wind direction (Fig. 3). The sharp edges of the roof-corner are fixed lines of flow separation, which produce vortex sheets that roll up to from the conical vortices. These vortices expand radially along their central axes in the neighborhood of the corner. The quasi-symmetry of this with respect to the bisector − perfect local symmetry is precluded by the fact that $\theta \neq 45^{o}$ and by the turbulence embedded within the incident wind − is responsible for the generation of these roof-corner vortices, so it follows that it should be reflected also in the character of the time-varying pressure field near the roof-corner.

In general, the control-point pdfs from V6 and V8 tend to exhibit greater variance (i.e., broader, less defined peaks) than those from V1. This is believed to be a manifestation of turbulent mixing in the roof-corner vortices, such that the downstream transducers (e.g., V6 and V8) are exposed to flow in which the turbulent energy has been spread across a broader range of scales than in the flow over V1. The vortical mixing severely alters the local character of coherent structures present in the

incident flow, and thus increases the variation in the associated pressure transients.

4. Conclusions

A wavelet-based, multi-scale detection and classification algorithm was designed to facilitate the analysis of intermittent, or transient-dominated, time series, with the ultimate goal of perceiving underlying structure in the detected transients. The joint time-scale localization built into the wavelet transform allows transients to be readily detected by choosing to retain portions of the signal in which the magnitudes of wavelet coefficients exceed a pre-specified threshold across contiguous scales.

The algorithm was applied to several intermittent pressure time series measured on the roof-corner of a low-rise building. The detected transients were sorted into three or four classes according to the number of suction peaks exhibited by smoothed versions of the original patterns. Class-dependent probability density functions were estimated nonparametrically for several features that summarize the shape of each transient.

The detection and classification algorithm provide quantitative insight into the characteristics of intermitternt pressure time series, particularly those associated with roofs of low-rise buildigns in quartering winds. In the published literature, there does not appear to have been a concerted effort to examine the statistics of individual pressure transients as distinct entities, even though they are responsible for generating the peak loads on structures subjected to intermittent wind loads; therefore, an immediate application of the algorithm would be to develop a database of wind pressure transients measured on the roofs of low-rise buildings. From this database, sufficient statistical information regarding transient loads could be extracted to improve or fine-tune existing design codes. Furthermore, with appropriate upstream flow measurements, analysis of individual transients could be used to enhance understanding of the mechanics by which these loads are created.

A related use would be to improve the fidelity of wind-tunnel modeling, especially in the simulation of intermittent turbulent flows. Current wind-tunnel procedure emphasizes primarily the scaled reproduction of turbulence spectra observed in the field, a practice that is predicated on the stationarity of the flow. Unfortunately, atmospheric flows are rarely stationary, so it is suggested that an extensive statistical description of the types of transients that should be reproduced could yield more insight into the quality of the wind tunnel modeling process.

References

Baxter, M.J. and Beardah, C.C. (1995), “Beyond the histogram-improved approaches to simple data display in archaeoloty using kernel density estimation”, *http://euler.ntu.ac.uk/ccb/html/densest.html*.

Daubechies, I. (1992), *Ten Lectures on Wavelets*, SIAM.

Daubechies, I. (1993), “Wavelet transforms and orthonormal wavelet bases”, *Different perspectives on wavelets (Proc. Symposia in Applied Mathematics)*, **46**, 1-33.

Dunyak, I, and others. (1998), “Coherent gust detection by wavelet transform”, *Journal of Wind Engineering and Industrial Aerodynamics*, **77-78**, 467-478.

Gilliam, X. and others. (1997), “Identification of coherent structure by wavelet analysis”, *Proceedings of Twelfth Conference on Boundary Layers and Turbulence*, 188-189.

Gurley, K. and Kareem, A. (1998), “On the analysis and simulation of random processes utilizing higher order spectra and wavelet transforms”, *Computational Stochastic Mechanics*, 315-324.

ICWE (1999), *Proceedings from the 10th International Conference on Wind Engineering*, Copenhagen, Denmark.
Jang, J.S.R., Sun, C. T. and Mizutani, E. (1997), *Neuro-fuzzy and Soft Computing*, Prentice-Hall.
Jordan, D., Hajj, M.R. and Tieleman, H.W. (1996), "Resolution of turbulence scales in incident wind by continuous wavelet analysis", *Third International Colloquium on Bluff Body Aerodynamics and Applications.*
Kadambe, S. and Boudreaus-Bartels, G.F. (1992), "Application of the wavelet transform for piitch detection of speech signals", *IEEE Transactions on Information Theory*, **38**, 917-924.
Kaiser, G. (1994), *A Friendly Guide to Wavelets*. Birkhauser.
Levitan, M.L. and Mehta, K.C. (1992), "Texas tech field experiments for wind loads, Part I: building and pressure measuring system", *Journal of Wind Engineering and Industrial Aerodynamics*, **41-44**, 1565-1576.
Levitan, M.L. and Mehta, K.C. (1992), "Texas tech field experiments for wind loads, Part II: meteorological instrumentation and terrain parameters", *Journal of Wind Engineering and Industrial Aerodynamics*, **41-44**, 1577-1588.
Lin, J.X., Surry, D. and Tieleman, H.W. (1995), "The distribution of pressure near roof corners of flat roof low buildings", *Journal of Wind Engineering and Industrial Aerodynamics*, **56**, 235-265..
Looney, C.G. (1998), *Pattern Recognition Using Neural Networks*. Oxford University Press.
Mallat, S. (1998), *A Wavelet Tour of Signal Processing*. Academic Press.
Ogden, R.T. (1997), *Essential Wavelets for Statistical Applications and Data Analysis*, Birkhauser.
Pettit, C.L. (1998), *Wavelet Analysis and Multi-scale Pattern Classification in Wind Engineering*, Ph.D. Dissertation, The Johns Hopkins University.
Pettit, C.L., Jones, N.P. and Ghane, R. (1998), "Analysis of pressure transients via wavelet analysis and pattern classification", *12th ASCE Engineering Mechanics Division Conference*, San Doego.
Strang, G. and Nguyen, T. (1996), *Wavelets and Filter Banks*, Wellesley-Cambridge Press.
Suhir, E. (1997), *Applied Probability for Engieers and Scientists*, Mc-Graw Hill.
Tieleman, H.W., Surry, D. and Lin. J.X. (1994), "Characteristics of mean and fluctuating pressure coefficients under corner (delta wing) vortices", *Journal of Wind Engineering and Industrial Aerodynamics*, **52**, 263-275.

(*Communicated by Ahsan Kareem*)